# Gene editing in a *Myo6* semi-dominant mouse model rescues auditory function

Yuanyuan Xue,[1,2,3,16] Xinde Hu,[4,5,16] Daqi Wang,[1,2,3,16] Di Li,[6,15,16] Yige Li,[7] Fang Wang,[1,2,3] Mingqian Huang,[8,9] Xi Gu,[1,2,3] Zhijiao Xu,[1,2,3] Jinan Zhou,[1,2,3] Jinghan Wang,[1,2,3] Renjie Chai,[7,10,11] Jun Shen,[12,13] Zheng-Yi Chen,[8,9] Geng-Lin Li,[1,3] Hui Yang,[5] Huawei Li,[1,2,3,14,17] Erwei Zuo,[6,17] and Yilai Shu[1,2,3,17]

[1]ENT Institute and Department of Otorhinolaryngology, Eye & ENT Hospital, State Key Laboratory of Medical Neurobiology and MOE Frontiers Center for Brain Science, Fudan University, Shanghai 200031, China; [2]Institutes of Biomedical Sciences, Fudan University, Shanghai 200032, China; [3]NHC Key Laboratory of Hearing Medicine, Fudan University, Shanghai 200031, China; [4]Institute of Neuroscience, State Key Laboratory of Neuroscience, Key Laboratory of Primate Neurobiology, CAS Center for Excellence in Brain Science and Intelligence Technology, Shanghai Research Center for Brain Science and Brain-Inspired Intelligence, Shanghai Institutes for Biological Sciences, Chinese Academy of Sciences, Shanghai 200031, China; [5]College of Life Sciences, University of Chinese Academy of Sciences, Beijing 100049, China; [6]Shenzhen Branch, Guangdong Laboratory for Lingnan Modern Agriculture, Genome Analysis Laboratory of the Ministry of Agriculture, Agricultural Genomics Institute at Shenzhen, Chinese Academy of Agricultural Sciences, Shenzhen 518124, China; [7]MOE Key Laboratory for Developmental Genes and Human Disease, School of Life Sciences and Technology, Jiangsu Province High-Tech Key Laboratory for Bio-Medical Research, Southeast University, Nanjing 210096, China; [8]Department of Otolaryngology-Head and Neck Surgery, Graduate Program in Speech and Hearing Bioscience and Technology and Program in Neuroscience, Harvard Medical School, Boston, MA 02115, USA; [9]Eaton-Peabody Laboratory, Massachusetts Eye and Ear Infirmary, Boston, MA 02114, USA; [10]Co-Innovation Center of Neuroregeneration, Nantong University, Nantong 226001, China; [11]Institute for Stem Cell and Regeneration, Chinese Academy of Science, Beijing, Shanghai 200032, China; [12]Department of Pathology, Brigham and Women's Hospital, Harvard Medical School, Boston, MA 02115, USA; [13]Harvard Medical School Center for Hereditary Deafness, Boston, MA 02115, USA; [14]The Institutes of Brain Science and the Collaborative Innovation Center for Brain Science, Fudan University, Shanghai 200032, China; [15]State Key Lab for Conservation and Utilization of Subtropical Agric-Biological Resources, Guangxi University, Nanning 530005, China

**Myosin VI（MYO6）is an unconventional myosin that is vital for auditory and vestibular function. Pathogenic variants in the human *MYO6* gene cause autosomal-dominant or -recessive forms of hearing loss. Effective treatments for *Myo6* mutation causing hearing loss are limited. We studied whether adeno-associated virus (AAV)-PHP.eB vector-mediated *in vivo* delivery of *Staphylococcus aureus* Cas9 (SaCas9-KKH)-single-guide RNA (sgRNA) complexes could ameliorate hearing loss in a *Myo6*$^{WT/C442Y}$ mouse model that recapitulated the phenotypes of human patients. The *in vivo* editing efficiency of the AAV-SaCas9-KKH-Myo6-g2 system on *Myo6*$^{C442Y}$ is 4.05% on average in *Myo6*$^{WT/C442Y}$ mice, which was ∼17-fold greater than editing efficiency of *Myo6*$^{WT}$ alleles. Rescue of auditory function was observed up to 5 months post AAV-SaCas9-KKH-Myo6-g2 injection in *Myo6*$^{WT/C442Y}$ mice. Meanwhile, shorter latencies of auditory brainstem response (ABR) wave I, lower distortion product otoacoustic emission (DPOAE) thresholds, increased cell survival rates, more regular hair bundle morphology, and recovery of inward calcium levels were also observed in the AAV-SaCas9-KKH-Myo6-g2-treated ears compared to untreated ears. These findings provide further reference for *in vivo* genome editing as a therapeutic treatment for various semi-dominant forms of hearing loss and other semi-dominant diseases.**

## INTRODUCTION

MYO6 is an unconventional myosin of 1,265 amino acids.[1] It consists of an N-terminal motor domain that is involved in actin bind-ing and movement, a calmodulin-interacting neck domain, and a C-terminal tail domain that often connects to various cargo-associated proteins.[2] MYO6 is expressed in the hair cells of the inner ear and is localized to the base of the stereocilia in the cuticular plate and thus is assumed to play important roles in anchoring the stereocilia to the cuticular plate.[3] Pathogenic variants in the *MYO6* gene can cause either autosomal dominant inherited non-syndromic hearing loss (DFNA22) or autosomal recessive inherited non-syndromic hearing loss (DFNB37).[3–7] Recently, a large-scale genetic analysis of Japanese patients with hearing loss found that 2.4% of autosomal dominant sensorineural hearing loss cases were caused by *MYO6* mutations.[8]

The MYO6 p.C442Y mutation causes DFNA22. Carriers of the $Myo6^{C442Y}$ mutation begin to develop progressive hearing loss during childhood and show profound sensorineural hearing loss by middle age.[5] We previously established a $Myo6^{WT/C442Y}$ mouse model that recapitulates postlingual progressive sensorineural deafness in humans. This mouse model exhibits hearing loss starting from 3 weeks after birth and progresses to profound deafness accompanied by degeneration of hair cells and disorganization of the stereocilia in the organ of Corti with a semi-dominant inheritance pattern.[9] Although MYO6 mutations are known to play an important role in hereditary deafness, currently there is still a lack of effective treatment and prevention methods.

Gene therapy holds a promise for treating hearing loss or promoting the survival of spiral ganglion neurons after injury,[10] and multiple preclinical trials of adeno-associated virus (AAV)-mediated gene overexpression therapy in recessive mouse models of human forms of deafness have reported successful prevention of hearing impairment.[11–19] However, such strategies have the disadvantages of a short time window for their effectiveness and a lack of controlled gene expression,[20] and such therapies might not be appropriate for semi-dominant inheritance mutations like that seen for MYO6 p.C442Y. Fortunately, the CRISPR-Cas9 (clustered regularly interspaced short palindromic repeats, CRISPR-associated protein 9) system provides a powerful genome-editing tool that can precisely correct mutations in the inner ear.[21–24]

MYO6 is expressed in both outer hair cells (OHCs) and inner hair cells (IHCs), particularly at the base of the stereocilia in the cuticular plate.[3,4] Further studies also revealed that MYO6 is involved in the morphological and functional maturation of IHC ribbon synapses and is required for efficient $Ca^{2+}$-dependent exocytosis.[4,25] Several Myo6 mutations are known to exhibit an autosomal recessive inheritance pattern.[1,6,26,27] For instance, an intronic point mutation (IVS5 G>A) results in skipping of exon 5 (130 bp) from the Myo6 transcript and results in a frameshift that introduces a stop codon at amino acid 95. Auditory brainstem response (ABR) testing showed that this heterozygous mutation had similar hearing threshold levels as wild-type (WT) mice when tested at 4, 8, and 24 weeks of age.[27] One $Myo6^{WT}$ allele appears to be sufficient to maintain normal hearing, and we hypothesized that specifically knocking out the mutated $Myo6^{C442Y}$ allele in heterozygous $Myo6^{WT/C442Y}$ mice can restore hearing.

In order to verify this hypothesis, the $Myo6^{C442Y}$ allele was specifically knocked out using SaCas9-KKH and a newly identified and highly efficient AAV-PHP.eB delivery system for hair cells.[28] The results demonstrated that knocking out the $Myo6^{C442Y}$ mutant allele could rescue hearing loss, and these observations support the use of this therapeutic strategy for most other semi-dominant diseases.

## RESULTS

### Specific disruption of the $Myo6^{C442Y}$ allele in vitro using SaCas9-KKH

The $Myo6^{WT/C442Y}$ mice have a G to A change (NM_001039546.1: c.1325G>A), and Cas9 must distinguish the $Myo6^{C442Y}$ allele from

the $Myo6^{WT}$ allele; the shorter SaCas9-KKH was chosen to enable successful packaging within one AAV vector. Two sgRNAs were designed to specifically target the mutant $Myo6^{C442Y}$ allele (Figure 1A). In order to evaluate the allele specificity of the genomic DNA modification, we performed lipid-mediated delivery of the Cas9-sgRNA-GFP plasmid into cultured mouse embryonic stem cells (mESCs) derived from $Myo6^{WT/WT}$, $Myo6^{WT/C442Y}$, and $Myo6^{C442Y/C442Y}$ mice (Figure 1B). The sgRNA target site was amplified by PCR, and the editing efficiency was analyzed by next-generation sequencing (NGS).

A higher rate of targeted insertions or deletions (indels) in mutant $Myo6^{C442Y/C442Y}$ mESCs (23.22% ± 1.76%) was observed with Myo6-g2 compared to Myo6-g1 (0.27% ± 0.06%) (Figure 1C). The Myo6-g2 editing efficiency of the $Myo6^{C442Y}$ allele in $Myo6^{C442Y/C442Y}$ was ~21-fold greater than editing efficiency of the $Myo6^{WT}$ allele (1.13% ± 0.25%) in $Myo6^{WT/WT}$ mESCs. The editing efficiency of Myo6-g2 was also higher for the $Myo6^{C442Y}$ allele in $Myo6^{WT/C442Y}$ mESCs (23.7% ± 2.04%) than that of Myo6-g1 (0.06% ± 0.04%) (Figure 1D). The Myo6-g2 editing efficiency of the $Myo6^{C442Y}$ allele in $Myo6^{WT/C442Y}$ was ~19-fold greater than editing efficiency of the $Myo6^{WT}$ allele (1.23% ± 0.25%) in $Myo6^{WT/C442Y}$ mESCs. Myo6-g2 specifically edited $Myo6^{C442Y}$ alleles both in $Myo6^{C442Y/C442Y}$ and $Myo6^{WT/C442Y}$ mice, which is consistent with the report that the 1-bp mismatch in the protospacer adjacent motif (PAM) was sufficient to distinguish between the mutant and WT alleles.[22] The indel profile indicated that majority of the Myo6-g2-induced variants were deletions, and the frameshift mutation ratios were 83.3% (Figures 1E and 1F; Data S1). In the in silico off-target analysis of Myo6-g2 using the Cas-OFFinder software,[29] we examined up to 15 off-target sites in mESCs transfected with Myo6-g2 or control sgRNA (non-targeted sgRNA, NT-sg), and no obvious indel mutations were observed (Figure 1G; Data S2). These results suggested that SaCas9-KKH-Myo6-g2 was a better strategy when compared to SaCas9-KKH-Myo6-g1, and SaCas9-KKH-Myo6-g2 was used in the subsequent in vivo experiments.

### In vivo genome editing with SaCas9-KKH-Myo6-g2

SaCas9-KKH-Myo6-g2 was packaged into AAV-PHP.eB, which was reported in our previous work to be highly effective at infecting hair cells (Figure S1).[28] The AAV-SaCas9-KKH-Myo6-g2 was injected into the inner ears of $Myo6^{C442Y/C442Y}$, $Myo6^{WT/C442Y}$, and $Myo6^{WT/WT}$ post-natal day (P) 0–2 mice (Figure 2A).

PCR products of target sites were analyzed by NGS at P14, and we observed an indel frequency of 3.51% ± 3.12% in AAV-SaCas9-KKH-Myo6-g2-treated $Myo6^{C442Y/C442Y}$ ears but effectively no indels (0.01%) in the untreated ears (Figure 2B). For $Myo6^{WT/WT}$ mice, there was no significant difference in indel frequency between the AAV-SaCas9-KKH-Myo6-g2-treated and untreated groups (0.015% for treated versus 0.012% for untreated), which was consistent with the in vitro results in Figure 1C. In $Myo6^{WT/C442Y}$ mice, Myo6-g2 edited the $Myo6^{C442Y}$ alleles specifically (4.05% ± 2.38% from six independent cochlea), which was ~17-fold greater than the editing efficiency
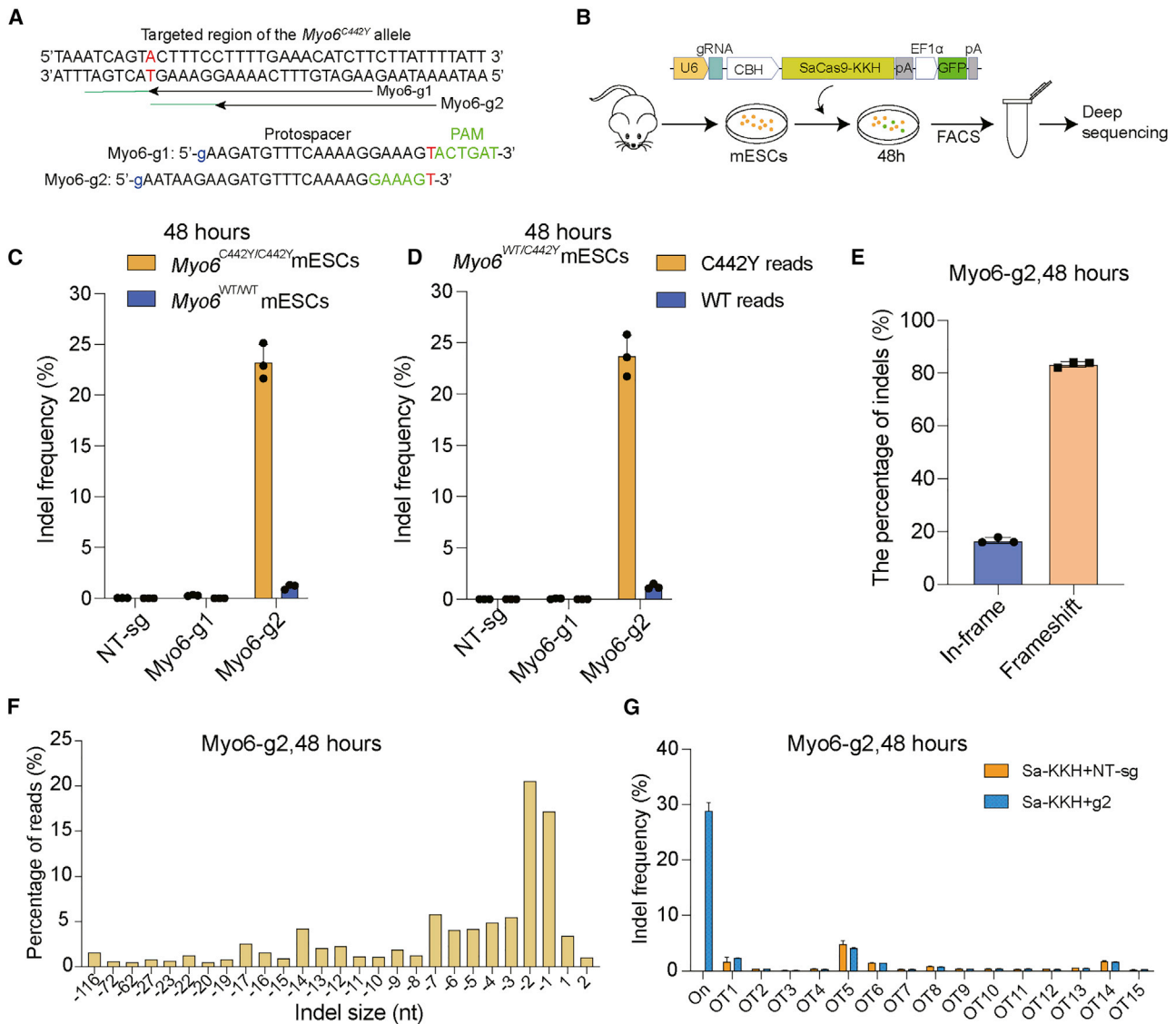
**Figure 1. The genome-editing strategy to disrupt the *Myo6*<sup>C442Y</sup> mutant allele**

(A) SaCas9-KKH sgRNA design. The *Myo6* p.C442Y mutation site is highlighted in red (a G to A transition at position 1325 of the *Myo6* cDNA). Nucleotides of the PAM sites are marked by green. (B) Schematic for the *in vitro* studies in *Myo6*<sup>C442Y/C442Y</sup> ESCs. Lipofectamine 3000-mediated delivery of the SaCas9-KKH sgRNA therapy vector into ESCs. Cells were sorted by GFP expression. (C and D) Indel percentages of g1 and g2 in *Myo6*<sup>WT/WT</sup>, *Myo6*<sup>C442/C442Y</sup>, and *Myo6*<sup>WT/C442Y</sup> mESCs were determined by targeted NGS and analysis using Seqkit. Individual values (n = 3) are shown, and horizontal lines and error bars represent the mean values ± SD of three independent biological replicates. Each dot represents the DNA from one sample. (E) The indels causing in-frame versus frameshift mutations were calculated after SaCas9-KKH-Myo6-g2 transfection in *Myo6*<sup>C442Y/C442Y</sup> ESCs. The data were obtained from the average of three independent repeated experiments. (F) Indel profiles from SaCas9-KKH-Myo6-g2-transfected *Myo6*<sup>C442Y/C442Y</sup> ESCs. Negative numbers represent deletions, and positive numbers represent insertions. Sequences without indels (value = 0) are not included in the chart. (G) Indel frequency at the *Myo6*<sup>C442Y</sup> mutation locus (On) and at each of the off-target (OT) loci in SaCas9-KKH-Myo6-g2-treated *Myo6*<sup>C442Y/C442Y</sup> ESCs. Blue, samples treated with DNA plasmids encoding SaCas9-KKH-Myo6-g2; orange, control samples with SaCas9-KKH-Myo6-NT-sg.

of *Myo6*<sup>WT</sup> alleles (0.24% ± 0.16% from four independent cochlea) (Figure 2C and Data S1).

The indel profile showed that the majority of AAV-SaCas9-KKH-Myo6-g2-induced variants in the *Myo6*<sup>C442Y</sup> allele were deletions, and the frameshift mutation rates were 89.0% and 92.3% for

*Myo6*<sup>C442Y/C442Y</sup> and *Myo6*<sup>WT/C442Y</sup>, respectively (Figure 2D). The most common mutation variants were −1 bp (0.81%/3,690 reads in *Myo6*<sup>WT/C442Y</sup>, 0.64%/7,221 reads in *Myo6*<sup>C442Y/C442Y</sup>), −2 bp (0.89%/ 4,077 reads in *Myo6*<sup>WT/C442Y</sup>, 0.56%/6,328 reads in *Myo6*<sup>C442Y/C442Y</sup>), and +1 bp (0.51%/2,350 reads in *Myo6*<sup>WT/C442Y</sup>, 0.28%/3,115 reads in *Myo6*<sup>C442Y/C442Y</sup>) frameshifts (Figures 2E and 2F; Data S1).
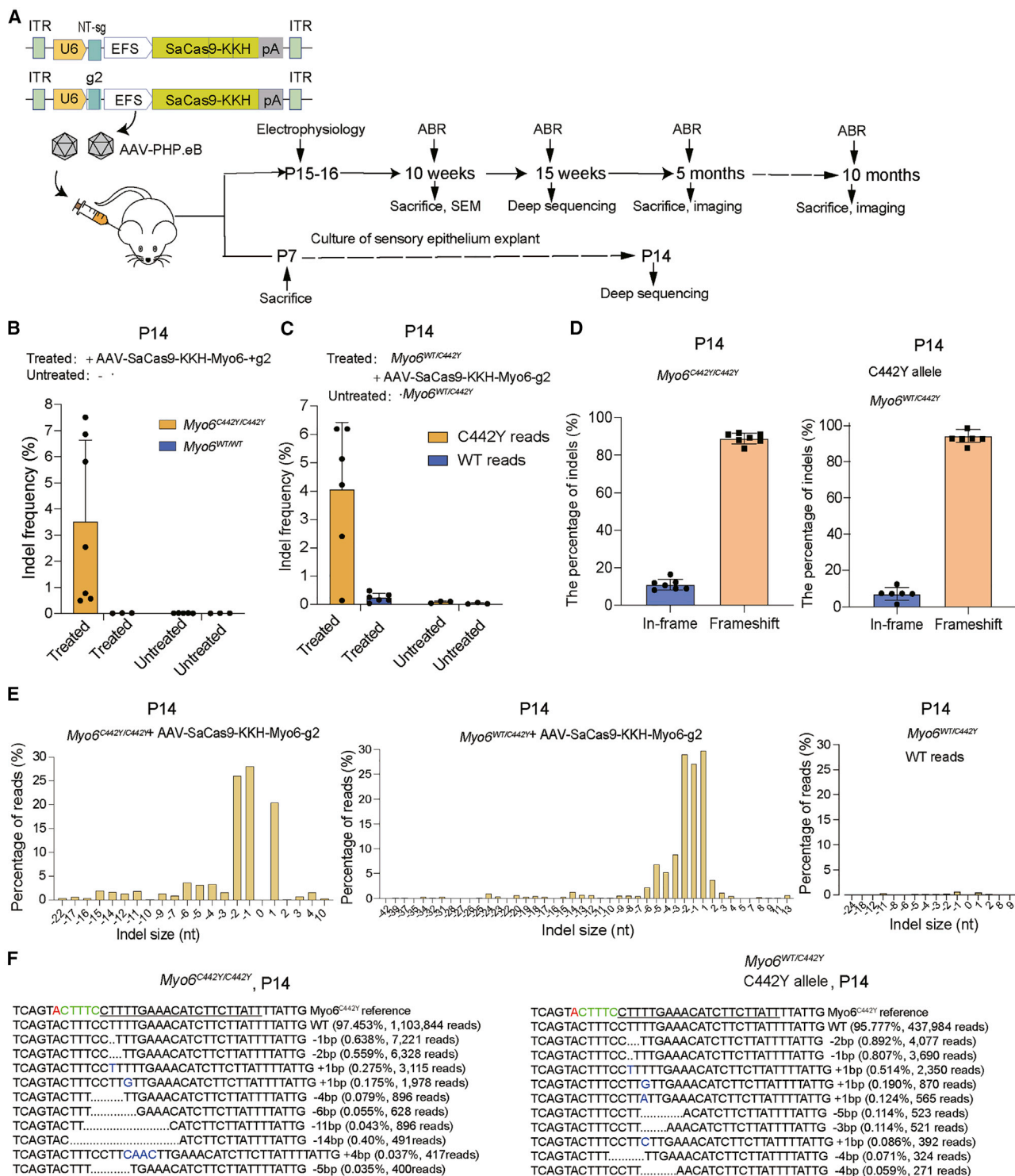
**Figure 2. *In vivo* genome editing with the AAV.PHP.eB-SaCas9-KKH-Myo6-g2 system**

(A) Schematic of the AAV vectors (control and g2) and the experimental overview of the *in vivo* studies. (B and C) The indel percentages at P14 in *Myo6^C442Y/C442Y^*, *Myo6^WT/C442Y^*, and *Myo6^WT/WT^* in the sensory epithelia were determined by targeted NGS. The samples were from ears treated with or without AAV.PHP.eB-SaCas9-KKH-Myo6-g2 at P0–2 via

*(legend continued on next page)*

In AAV-SaCas9-KKH-Myo6-g2-treated $Myo6^{WT/C442Y}$ mice, we also observed indel formation for $Myo6^{C442Y}$ alleles at the mRNA level at P15 (0.8% ± 0.01%), which was ~10-fold greater than the editing efficiency of the $Myo6^{WT}$ alleles (0.08%; Figure S2A). We observed the proportion of $Myo6^{C442Y}$ mRNA allele reads decreased in the treated group relative to the untreated group (51.3% versus 52.4%, n = 4) (Figure S2B).

In order to determine whether the gene editing was stable for a long time, we chose 15 weeks, which is one of the best time points for hearing rescue performance according to our study, to analyze the gene-editing efficacy. Because the sensory epithelium is difficult to separate at 15 weeks, the whole soft cochlear tissue was used instead. In the whole cochlea, in which supporting cells vastly outnumber the AAV-SaCas9-KKH-Myo6-g2-targeted hair cells, we could still observe an indel frequency of 3.63%, which was similar to 4.05% at P14. However, editing in WT alleles was also observed (0.17%; Figure S3), which was consistent with a previous report.[22] This might be caused by the inability of the single G or A to accurately distinguish the $Myo6^{WT}$ from $Myo6^{C442Y}$ allele for indel analysis. However, the ratio of indel frequencies in AAV-SaCas9-KKH-Myo6-g2-treated $Myo6^{WT}$ alleles and untreated $Myo6^{WT}$ (background) was not increased even after 15 weeks (6.36-fold at P14 versus 2.62-fold at 15 weeks) (Figure 2C; Figure S3; Data S1). These results indicated that AAV-SaCas9-KKH-Myo6-g2 could specifically edit the $Myo6^{C442Y}$ alleles in vivo for a long time.

### Allele-specific knockout of $Myo6^{C442Y}$ improves hearing function

To study the effect of the AAV-SaCas9-KKH-Myo6-g2 system on hearing function in $Myo6^{WT/C442Y}$ mice, we recorded ABRs, which represent the sound-evoked neural output of the cochlea from treated and untreated ears to evaluate the extent of hearing recovery across frequencies ranging from 4 kHz to 32 kHz. We first evaluated whether the injection of the vectors affected hearing function. We found that there was no ABR threshold elevation in the AAV-SaCas9-KKH-Myo6-g2-treated ears compared with the untreated ears (16 kHz: treated, 31.1 ± 1.8 dB, n = 9; untreated, 31.1 ± 1.8 dB, n = 9, p > 0.05) in $Myo6^{WT/WT}$ mice (Figure S4A). No hair cell loss was detected along the tonotopic axis of the cochlea in the AAV-SaCas9-KKH-Myo6-g2-treated group (Figures S4B and S4C; p > 0.05), which confirmed that the AAV-SaCas9-KKH-Myo6-g2 therapeutic system does not affect the hearing function of WT mice.

At 10 weeks, the ABR thresholds were significantly decreased at all the tested frequencies in AAV-SaCas9-KKH-Myo6-g2-treated ears compared to the untreated ears (16 kHz: treated, 43.3 ± 2.7 dB, n = 26; untreated, 65.2 ± 3.8 dB, n = 26, p < 0.0001) (Figure 3A). The wave 1 latencies stimulated by 90 dB SPL (sound pressure level) sound at 8 kHz and 16 kHz were shorter in the AAV-SaCas9-KKH-Myo6-g2-treated ears compared to the untreated ears (8 kHz: treated,

1.9 ± 0.1 ms, n = 15; untreated, 2.4 ± 0.1 ms, n = 13, p < 0.01; 16 kHz: treated, 1.8 ± 0 ms, n = 15; untreated, 2.5 ± 0.1 ms, n = 15, p < 0.0001) (Figure 3B), but we did not detect significant changes in ABR wave I amplitudes in the AAV-SaCas9-KKH-Myo6-g2-treated ears compared with the untreated ears at 10 weeks (Figure 3C).
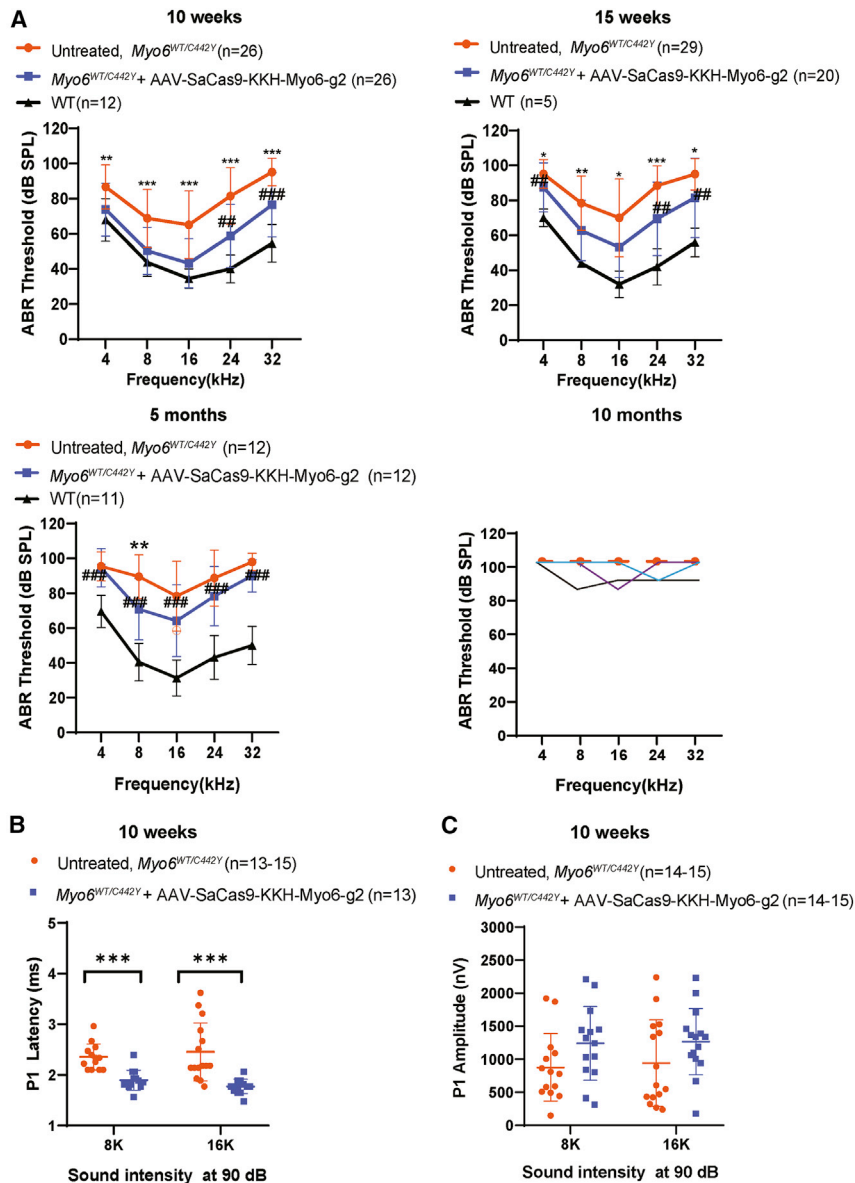
At 15 weeks, the ABR thresholds were also significantly decreased in AAV-SaCas9-KKH-Myo6-g2-treated ears compared to the untreated ears (16 kHz: treated, 53.3 ± 17.3 dB, n = 20; untreated, 70 ± 22.2 dB, n = 29, p < 0.0001) (Figure 3A). However, the magnitude of the improvement at 5 months was reduced at 4 out of 5 frequencies and persisted only at 8 kHz (treated, 70.8 ± 17.7 dB, n = 12; untreated, 89.6 ± 12.5 dB, n = 12, p < 0.01) (Figure 3A). With continuous observation up to 10 months, untreated $Myo6^{WT/C442Y}$ mice showed no detectable ABR thresholds, indicating profound deafness. In contrast, 3 out of 5 mice showed mild hearing improvements in the AAV-SaCas9-KKH-Myo6-g2-treated group (Figure 3A).

From the ABR threshold comparison between WT controls and AAV-SaCas9-KKH-Myo6-g2-treated $Myo6^{WT/C442Y}$ ears, there also appeared to be significant differences at 24 kHz and 32 kHz at 10 weeks; at 4 kHz, 24 kHz, and 32 kHz at 15 weeks; and at all frequencies at 5 months. There was significant hearing loss at 5 months. The ABR thresholds of individual mice at 10 weeks, 15 weeks, 5 months, and 10 months are shown in Figure S5, which indicates the variations in individual hearing function in semi-dominant mouse models. The results demonstrated that knocking out the $Myo6^{C442Y}$ mutant allele could initially improve auditory function, but the auditory function began to decline at 5 months, and by 10 months the auditory performance was severely degraded. It is likely that the waning of ABR thresholds at 10 months was a continuation of the decline in responsivity seen at 5 months.

In contrast with the injection of AAV-SaCas9-KKH-Myo6-g2, none of the mice treated with the control AAV-SaCas9-KKH virus recovered auditory function at 10–12 weeks (16 kHz: treated, 62.5 ± 20.7 dB, n = 10; untreated, 65 ± 20.1 dB, n = 10, p > 0.05) (Figure S6A), and the hair cell survival rate was also not improved in the AAV-SaCas9-KKH-treated group (p > 0.05 at all tested frequencies) (Figures S6B and S6C). This suggested that the specific gene editing is necessary for auditory rescue.

We also found that the DPOAE thresholds in AAV-SaCas9-KKH-Myo6-g2-treated $Myo6^{WT/C442Y}$ mice showed recovery at 5, 10, and 12 weeks (Figure S7), which reflected the recovery of OHCs' amplification function. At 10 weeks, the DPOAE threshold of the AAV-SaCas9-KKH-Myo6-g2-treated ears was significantly decreased at 8 kHz and 16 kHz compared with the untreated ears.

---

the scala media (n = 3–7). Data are presented as the mean ± SD. (D) The indels causing in-frame versus frameshift mutations were calculated after AAV.PHP.eB-SaCas9-KKH-Myo6-g2 infection in $Myo6^{C442Y/C442Y}$ and $Myo6^{WT/C442Y}$ mice. (E) Indel profiles from SaCas9-KKH-Myo6-g2-transfected $Myo6^{C442Y/C442Y}$ and $Myo6^{WT/C442Y}$ mice. Negative numbers represent deletions, and positive numbers represent insertions. $Myo6^{C442Y}$ and $Myo6^{WT}$ reads are plotted separately. Sequences without indels (value = 0) are omitted from the chart. (F) The most abundant reads in the AAV.PHP.eB-SaCas9-KKH-Myo6-g2-treated $Myo6^{C442Y/C442Y}$ and $Myo6^{WT/C442Y}$ mice are shown.

**Figure 3. Effects of the AAV-PHP.eB-SaCas9-KKH-g2 virus on the inner ear ABR thresholds in Myo6^WT/C442Y mice**

(A) ABR thresholds in $Myo6^{WT/C442Y}$ ears treated with AAV.PHP.eB-SaCas9-KKH-Myo6-g2 (blue), untreated $Myo6^{WT/C442Y}$ ears (orange), and WT ears (black) after 10 weeks, 15 weeks, and 5 months. At 10 months, the dashed line of the same orange color denotes the mean data of untreated $Myo6^{WT/C442Y}$ ears, and the solid lines (purple, black, and blue) denote the three individual AAV-SaCas9-KKH-Myo6-g2-treated ears showing mild hearing improvement. Statistical analysis between untreated and AAV.PHP.eB-SaCas9-KKH-Myo6-g2-treated $Myo6^{WT/C442Y}$ ears was by one-way ANOVA: ***$p < 0.001$; **$p < 0.01$; *$p < 0.05$. The statistical analysis between WT and AAV.PHP.eB-SaCas9-KKH-Myo6-g2-treated $Myo6^{WT/C442Y}$ ears was by one-way ANOVA: ###$p < 0.001$; ##$p < 0.01$; #$p < 0.05$. Values and error bars reflect the mean ± SD. (B) Latency of ABR wave 1 at 8 kHz and 16 kHz at 10 weeks. (C) Amplitude of ABR wave 1 at 8 kHz and 16 kHz at 10 weeks. AAV.PHP.eB-SaCas9-KKH-Myo6-g2-treated $Myo6^{WT/C442Y}$ ears (blue) were compared with untreated $Myo6^{WT/C442Y}$ ears (orange). Values and error bars reflect the mean ± SEM. Statistical analysis was by unpaired two-tailed Student's t tests. ***$p < 0.001$.

tion of AAV-SaCas9-KKH-Myo6-g2 into the inner ears, but the effect was gradually lost over time.

## Allele-specific knockout of $Myo6^{C442Y}$ improves hair cell survival rates

$Myo6^{WT/C442Y}$ mice exhibited substantial degeneration of OHCs as previously described.[9] To assess the effect of gene editing by AAV-SaCas9-KKH-Myo6-g2 on hair cell survival, we counted the hair cells at 5 months and 10 months. At 5 months, the number of IHCs in $Myo6^{WT/C442Y}$ mice was not significantly different from WT, and the number of IHCs in the AAV-SaCas9-KKH-Myo6-g2-treated ears did not change (Figure 4A; Figures S4B and S6B). There were more OHCs in the AAV-SaCas9-KKH-Myo6-g2-treated ears (40.09 ± 0.34 and 35.18 ± 1.41 cells/100 μm in the middle and basal turns of the cochlea, respectively) than in the untreated ears (34.36 ± 0.98 and 17.73 ± 2.43 cells/100 μm in the middle and basal turns of the cochlea, respectively) (Figure 4B). The survival of OHCs was significantly enhanced in the middle and basal turns of the cochlea in the AAV-SaCas9-KKH-Myo6-g2-treated ears. Representative images of hair cells at 5 months are shown in Figure S8.

At 10 months, more IHCs in the middle and basal turns were observed in the AAV-SaCas9-KKH-Myo6-g2-treated ears (11.33 ± 0.55 and 6 ± 0.41 cells/100 μm in the middle and basal turns of the cochlea, respectively) than in the untreated ears (6.11 ± 0.98 and 1.11 ± 0.31 cells/100 μm in the middle and basal turns of the

The untreated ears showed almost no detectable DPOAE thresholds following 80 dB SPL stimulation at high-frequency ranges (24–32 kHz), while the treated ears showed detectable DPOAE thresholds. From the DPOAE threshold comparison between WT controls and AAV-SaCas9-KKH-Myo6-g2-treated $Myo6^{WT/C442Y}$, it seemed that OHC function in the treated group was still significantly different from that of WT mice. Although the ABR thresholds of the AAV-SaCas9-KKH-Myo6-g2-treated ears at 24–32 kHz were decreased significantly compared to the untreated ears (p < 0.05), the treated ears show mild DPOAE recovery at the corresponding frequencies. We suspect that the large improvement in ABR thresholds at 24–32 kHz in the treated ears might be mainly due to the protection of IHC function. Together, these results indicate that the auditory function of $Myo6^{WT/C442Y}$ was partially recovered by injec-
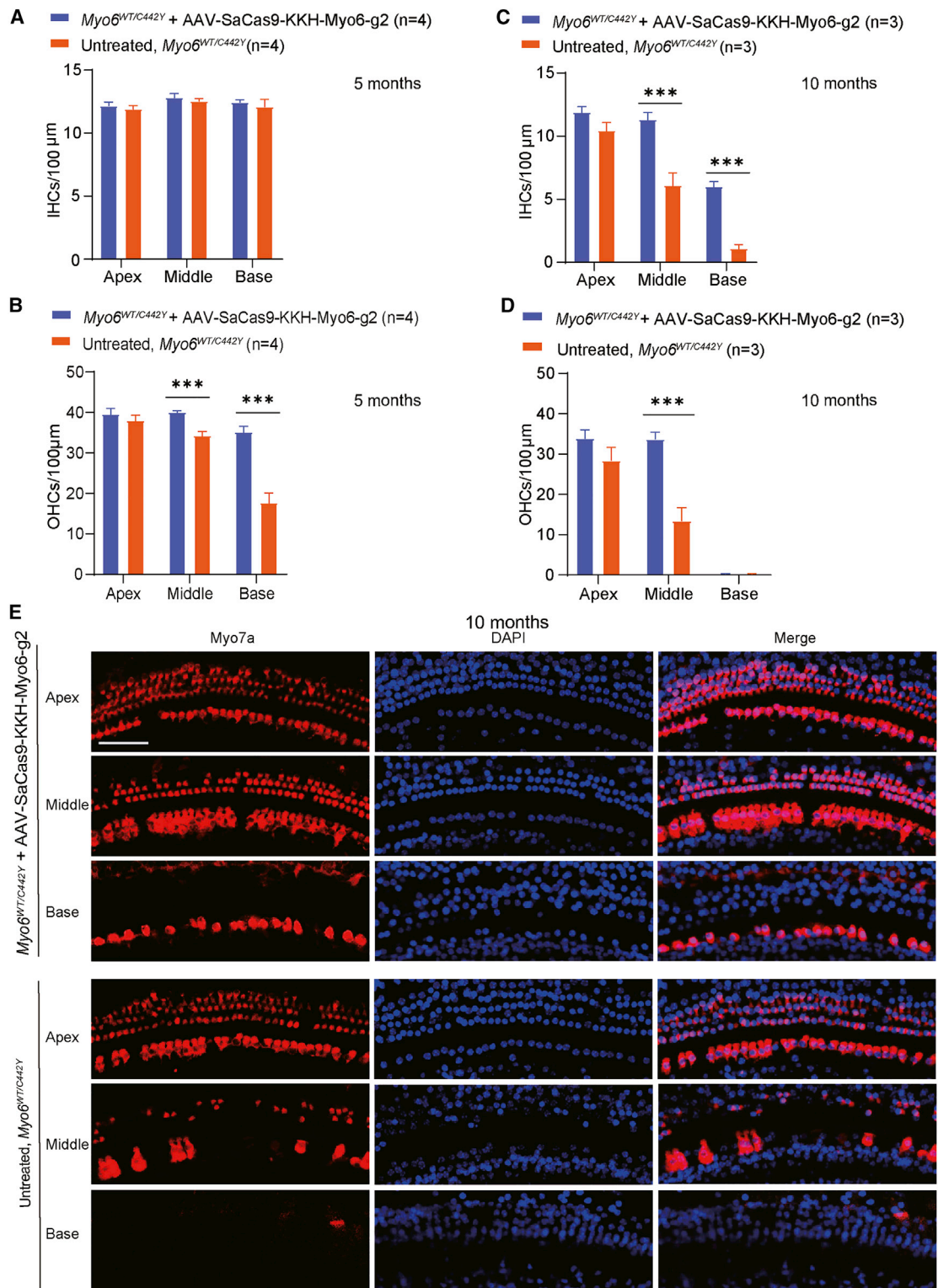
**Figure 4. Effects of the AAV-PHP.eB-SaCas9-KKH-g2 virus on cell survival rates in *Myo6^WT/C442Y* mice**

(A and B) The number of IHCs (A) and OHCs (B) per 100-μm section for four untreated and four AAV-PHP.eB-SaCas9-KKH-g2-treated *Myo6^WT/C442Y* cochleae from four mice at 5 months. (C and D) The numbers of IHCs (C) and OHCs (D) per 100-μm section for three untreated and three AAV-PHP.eB-SaCas9-KKH-g2-treated *Myo6^WT/C442Y*

*(legend continued on next page)*

cochlea, respectively) (Figures 4C and 4E). More OHCs were observed in the middle turn of the AAV-SaCas9-KKH-Myo6-g2-treated ears (33.78 ± 1.65 cells/100 μm) compared with untreated ears (13.44 ± 3.27 cells/100 μm) (Figures 4D and 4E). Almost no OHCs were observed in the basal turns of the two groups (Figure 4D). These results indicated that the survival rate of hair cells was significantly improved by knockout of the $Myo6^{C442Y}$ allele, and the hair cell loss in $Myo6^{WT/C442Y}$ mice progressed from OHCs to IHCs and from the basal turn to the apical turn.

### Allele-specific knockout of $Myo6^{C442Y}$ improves hair bundle morphology

Stereocilia bundles on hair cells are responsible for sound detection, and morphological defects in the stereocilia can cause deafness. In our previous study,[9] morphological abnormalities in cochlear hair bundles in $Myo6^{WT/C442Y}$ mice were observed at 6 weeks. Most hair bundles anchored on the remaining OHCs and IHCs retained normal morphology, but some were disorganized, with fused stereocilia and rotated polarity. At 12 weeks, the number of hair bundles in WT mice was approximately twice that of the $Myo6^{WT/C442Y}$ heterozygous mice along the middle and basal tonotopic axes. Thus, in present study the hair bundle morphology was evaluated by scanning electron microscopy in the AAV-SaCas9-KKH-Myo6-g2-treated and untreated ears of $Myo6^{WT/C442Y}$ mice at 10 weeks of age. In WT control ears, the hair bundles were arranged into two to three rows in a staircase pattern in OHCs and IHCs (Figure 5). In $Myo6^{WT/C442Y}$ mice, the surviving IHCs and OHCs showed significant disorganization, with fused stereocilia and rotated polarity in some regions, which was consistent with a previous report.[6] When AAV-SaCas9-KKH-Myo6-g2 was delivered into the $Myo6^{WT/C442Y}$ cochlea, we observed more organized hair bundles in OHCs and IHCs. The scanning electron microscopy results indicated that hair bundle defects caused by $Myo6^{WT/C442Y}$ mutation were amenable to restoration by injection of AAV-SaCas9-KKH-Myo6-g2.

### Electrophysiology showed recovery of IHC $Ca^{2+}$ current amplitudes after treatment with AAV-SaCas9-KKH-Myo6-g2

Previous studies have shown that knockout of $Myo6$ affects $Ca^{2+}$ current amplitude ($I_{Ca}$) and leads to capacitance changes in IHCs.[25,30] A net increase in whole-cell membrane capacitance ($\Delta C_m$) indicates sustained $Ca^{2+}$-dependent exocytosis of synaptic vesicles in IHCs, which will activate the auditory neuron. Therefore, we explored whether the $I_{Ca}$ and $\Delta C_m$ in IHCs of $Myo6^{WT/C442Y}$ mice were affected by SaCas9-KKH-Myo6-g2-mediated disruption of the $Myo6^{C442Y}$ allele. We isolated the apical turn of the sensory epithelium directly from the $Myo6^{WT/WT}$ and SaCas9-KKH-Myo6-g2-treated and untreated $Myo6^{WT/C442Y}$ cochleae at P15–16. We found that the $Myo6^{C442Y}$ mutation resulted in a decrease in $I_{Ca}$ current (WT ears, −235.1 ± 22.9 pA; untreated $Myo6^{WT/C442Y}$ ears, −145.8 ±

70.5 pA), and the $I_{Ca}$ of SaCas9-KKH-Myo6-g2-treated $Myo6^{WT/C442Y}$ ears was recovered to −194.3 ± 65.1 pA (Figures 6A and 6B). However, under our experimental conditions we found that the $Ca^{2+}$-induced exocytosis of IHCs from untreated mice was not affected by the $Myo6^{C442Y}$ mutation (WT ears, 115.4 ± 105.9 fF; untreated ears, 75.7 ± 57.6 fF, p > 0.05). For the treated $Myo6^{WT/C442Y}$ IHCs, the $\Delta C_m$ was 82.2 ± 71.9 fF (n = 26), which was not significantly different from WT (p > 0.05) (Figures 6C and 6D). The $\Delta C_m$ results indicated that the $Myo6^{C442Y}$ mutation did not affect the exocytosis of IHCs.

## DISCUSSION

In this study, we explored a possible treatment approach for $MYO6$ gene mutations, which are a frequent cause of autosomal-dominant hearing loss. We used a gene therapy system that included highly efficient hair-cell-targeting AAV.PHP.eB virus vector and CRISPR-SaCas9-KKH-Myo6-g2. The therapeutic system was delivered into $Myo6^{WT/C442Y}$ mouse ears at P0–2, where it specifically disrupted the $Myo6^{C442Y}$ mutant allele. Consequently, the genome editing specifically of $Myo6^{C442Y}$ alleles significantly improved the auditory function in $Myo6^{WT/C442Y}$ mice even though there was a marked decline from 5 months. This outcome together with previous reports of successful auditory restoration demonstrated the feasibility of gene therapy for hereditary deafness.[11–13,15–18,22–24,31–37] All of these preclinical gene therapy studies that have focused on different gene mutation sites will contribute to the development of precise treatments for deafness.[38]

Several factors were associated with the improvement in hearing seen in this work. First, it is widely accepted that OHCs are much more difficult to transfect with AAV compared to IHCs. Here, we used the highly infectious PHP.eB virus that even at a relatively low dose ensured that sufficient numbers of IHCs and OHCs would be transduced to enable assessment of whether or not there was rescue by the proposed strategy (Figure S1).[28] The high-titer AAVs AAV2.7m8, Anc80L65, and PHP.B have been fully studied in OHCs,[32,39–42] but this newly identified and highly efficient AAV-PHP.eB vector has not been previously used to deliver CRISPR-SaCas9 into the inner ear. Furthermore, the treatment approach via the scala media was found to be safe. Audiometry measurements and hair cell counting were performed 4 weeks after AAV-SaCas9-KKH-Myo6-g2 was injected into WT P0–2 mice, and no ABR threshold shifts or hair cell loss was observed, indicating that the injection of AAV-PHP.eB-SaCas9-KKH-g2 did not disrupt hearing function (Figures S4A–S4C). Finally, the progressive hearing loss in the $Myo6^{WT/C442Y}$ mouse model provided a sufficient treatment time window for P0–2 injection. According to a previous electrophysiology study of $Myo6^{sv/sv}$ mutant mice lacking $Myo6$ gene expression, ionic current and ribbon synapse maturation of IHCs could still proceed normally until P6,

---

cochleae from three mice at 10 months. Values and error bars reflect the mean ± SEM. Statistical analysis was by two-tailed Student's t tests. ***p < 0.001. NS, not significant. (E) Representative confocal images of cochleae harvested at 10 months from the AAV-PHP.eB-SaCas9-KKH-g2-treated and untreated ears of $Myo6^{WT/C442Y}$ mice. The apical, middle, and basal turns were dissected and stained with MYO7A (red) for hair cells and with DAPI (blue) for nuclei. Scale bar, 50 μm.
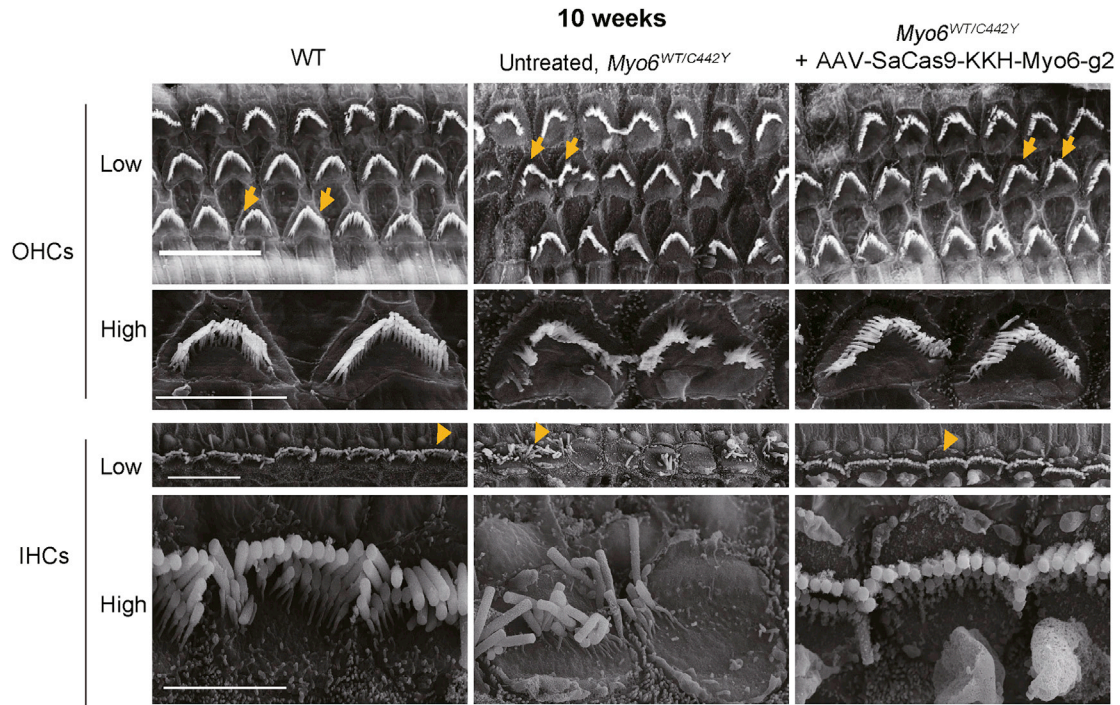
**Figure 5. Effects of the AAV-PHP.eB-SaCas9-KKH-g2 virus on hair bundle morphology of *Myo6^WT/C442Y* mice**

Scanning electron microscope images of the cochlea sensory epithelium showing the hair bundle morphology for untreated *Myo6^WT/WT* (left), untreated *Myo6^WT/C442Y* (middle), and AAV.PHP.eB-SaCas9-KKH-Myo6-g2-treated *Myo6^WT/C442Y* mice (right) at 10 weeks. Representative bundles (arrows) of OHCs and IHCs were enlarged in the corresponding lower panel. Scale bar in low-magnification figures, 10 μm. Scale bar in high-magnification figures, 4 μm. High, high magnification; Low, low magnification.

which indicated that the therapeutic time window of P0–2 we used to correct *Myo6^C442Y* mutation would be effective in mice.

In this study, the *in vitro* work for testing genome editing efficiency on mESCs was done using lipid-mediated delivery. It is well accepted that for genome editing efficiency studies, the specific values of guide RNA (gRNA) efficiency using lipid-mediated delivery or AAV-mediated delivery would be different. However, when we used the same delivery vector to compare different gRNA efficiencies in the same cell type, the sequence of gRNA was the main factor affecting the editing efficiency. Correspondingly, the highly efficient gRNAs screened using lipid-mediated delivery *in vitro* should also have relatively high editing efficiency *in vivo* when using an AAV-mediated delivery system.[43] Meanwhile, the use of lipid-mediated delivery systems for gRNA screening is well accepted in the field.[24]

We observed gene editing in all AAV-SaCas9-KKH-Myo6-g2-treated cochleae, and to a lesser extent in the contralateral ears of AAV-Sa-Cas9-KKH-Myo6-g2-treated mice, and this was likely because AAV vectors can diffuse to the contralateral ear of the same mouse through the cochlear aqueduct.[44]

It has been reported that MYO6 is located at the synaptic active zone of IHCs and is required for efficient Ca²⁺-dependent exocytosis in mature IHC ribbon synapses.[4,25] Therefore, we also focused on the $I_{Ca}$ and $\Delta C_m$ in IHCs to study the effect of the C442Y mutation in Myo6. Compared with WT mice, we found that the untreated *Myo6^WT/C442Y* inner ear showed decreased $I_{Ca}$, and AAV-SaCas9-KKH-Myo6-g2 treatment could rescue the decrease in $I_{Ca}$, which reflected the partially improved IHC function. We found that neither the exocytosis of IHCs (Figure 6D) nor the ABR wave I amplitude (Figure 3C) showed significant differences between treated and untreated ears. However, the two experiments were performed with extremely strong stimulation (500 ms voltage step to 0 mV, or 90 dB tone), which is likely to have obscured the subtle changes expected from the minimal and short stimulations used for determining the hearing thresholds. Our understanding of how the *Myo6^C442Y* mutation causes reduced electrophysiological performance is still very limited, and future work will help to fully understand the mechanisms behind these effects.

DPOAEs are an indicator of OHC function, and here we found that the DPOAE thresholds in AAV-SaCas9-KKH-Myo6-g2-treated *Myo6^WT/C442Y* mice showed partial recovery at 5, 10, and 12 weeks (Figure S7), which was not completely consistent with the ABR results. We also observed differences in the number of hair cells at 5 months and 10 months that also were not completely consistent with the ABR results. These observations suggest that the improvement of one index alone might not fully reflect the improvement of hearing function, and the improvement should instead be the result of the synergistic
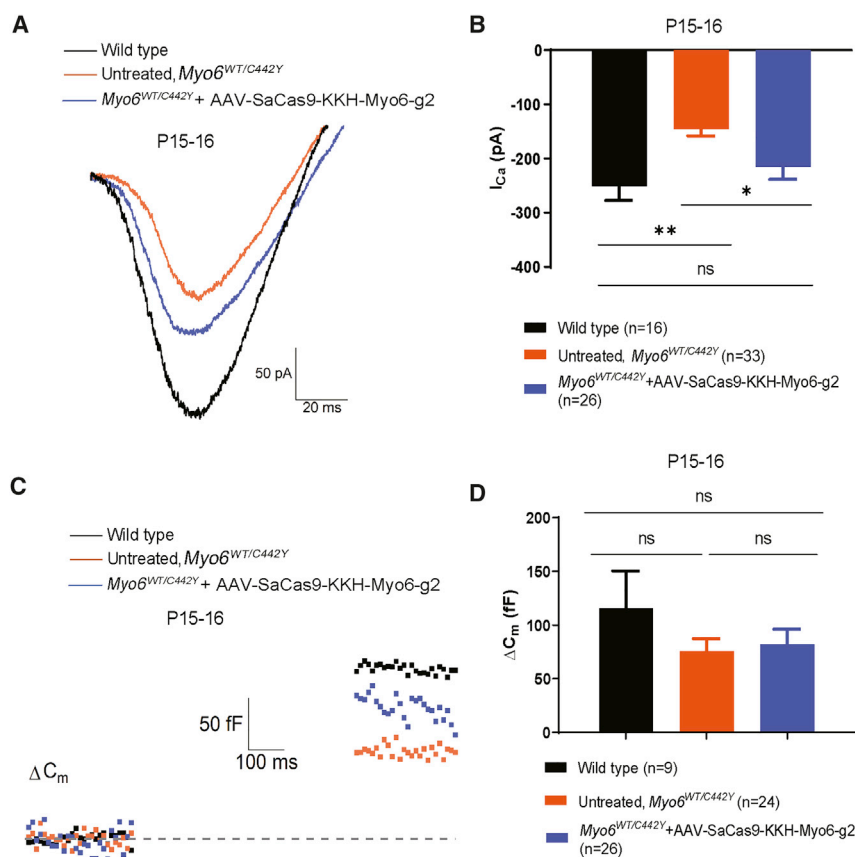
(A) Representative $I_{Ca}$ recordings in apical IHCs at P15–16 from untreated $Myo6^{WT/C442Y}$ mice (orange), WT mice (black), and $Myo6^{WT/C442Y}$ mice injected with AAV.PHP.eB-SaCas9-KKH-Myo6-g2 at P0–2 (blue). Untreated $Myo6^{WT/C442Y}$ = −150.84 pA. Treated $Myo6^{WT/C442Y}$ = −191.71 pA. WT = −291.77 pA. (B) $I_{Ca}$ values were recorded from a holding potential of −90 mV to +70 mV in 300 ms at P15–16 in IHCs from untreated ears (orange) and AAV.PHP.eB-SaCas9-KKH-Myo6-g2-treated ears (blue). Values and error bars reflect the mean ± SEM. Statistical analysis was by one-way ANOVA. **p < 0.01; *p < 0.05. (C) Representative $C_m$ measurements in IHCs, one from each group. Untreated $Myo6^{WT/C442Y}$ = 73.91 fF. AAV.PHP.eB-SaCas9-KKH-Myo6-g2-treated $Myo6^{WT/C442Y}$ = 96.46 fF. WT = 162.16 fF. (D) The net increase in $C_m$ before and after stimulation ($\Delta C_m$) was used to quantify exocytosis from the same IHCs as $I_{Ca}$. Values and error bars reflect the mean ± SEM. Statistical analysis was by one-way ANOVA. ns, not significant.

effect of several indexes. The morphological and physiological changes included increased hair cell numbers combined with partially rescued hair bundle arrangements in both IHCs and OHCs, partially recovered voltage-gated $Ca^{2+}$ current in IHCs, and recovered DPOAE in OHCs, and these are together likely to account for the overall hearing improvement we observed in AAV-SaCas9-KKH-Myo6-g2-treated ears.

Despite the positive results in our study, there were some limitations that should be noted. First, for the AAV-SaCas9-KKH-Myo6-g2 safety evaluation, 15 off-target sites were predicated by CasOFFinder and tested by NGS. Although CasOFFinder is widely accepted to predict off-target sites,[29] it is still necessary to further evaluate the specificity and safety of gRNA by genome-wide detection of off-target sites such as GUIDE-Seq, CIRCLE-seq, or GOTI before possible clinical application.[45,46] The second limitation of this study is that we analyzed only AAV-Cas9 infection of WT mice at 4 weeks but not at longer times. In this study, we found that knocking out the $Myo6^{C442Y}$ mutant allele improved auditory function initially, while the auditory function began to decline from 5 months onward, and the ABR performance was severely degraded to the untreated control level at 10 months. The phenomenon that auditory function decreases with time is common in previous other gene therapy studies of hearing loss.[23,37] It would be interesting and important to study the mechanism behind why the treatment effect declined with the prolongation

of time. On the one hand, the AAV-PHP.eB virus we used could efficiently infect the IHCs and the OHCs throughout the cochlea (Figure S1), it is possible that the gene editing efficiency for $Myo6^{C442Y}$ allele cannot rescue all mutations to maintain proper cellular function, and the ongoing, irreversible hair cell damage caused by mutation might be one of the possible reasons for this unsatisfactory situation. Our results indicated that improving the editing efficiency by optimizing or discovering new AAV-Cas9 therapy systems will potentially improve hearing more significantly and more consistently in the future. On the other hand, further studies of AAV-Cas9 infection of WT mice lasting 10 months or more are also required to confirm that AAV-SaCas9-KKH does not disrupt hearing function and that the hair cells can tolerate the expression of AAV-Cas9 for a long time, which would provide valuable information for illustrating the mechanism behind the phenomenon. Finally, it is important to note that neonatal mouse inner ears at P0–2, as used here, are only partially developed and continue to undergo structural maturation until the onset of hearing at P14–15.[47] The cochlea in P1–2 mice is temporally equivalent to the human cochlea prior to 26 weeks' gestational age,[48] so studies in older mice are needed before these findings can be translated to humans.

In conclusion, this study provides a proof of concept for *in vivo* genome editing as a therapeutic treatment for various semi-dominant forms of deafness and other semi-dominant human diseases.

## MATERIALS AND METHODS
### Animals
$Myo6^{WT/C442Y}$ and $Myo6^{C442Y/C442Y}$ ($Myo6^{WT/WT}$ as control) mice were established by Beijing Biocytogen.[9] Briefly, Cas9 mRNA and

sgRNAs along with the targeting vector containing the C442Y allele were microinjected into fertilized C57BL/6J oocytes to generate F0 founders. Since C57BL/6J mice have age-related hearing loss due to the homozygous $Cdh23^{ahl}$ allele, the Myo6-C442Y mice were crossed with CBA/CaJ mice, and offspring without $Cdh23^{ahl}$ were selected. Male and female Myo6-C442Y heterozygous mice were intercrossed to breed WT, heterozygous, and homozygous progenies. This animal study was approved by the Institutional Animal Care and Use Committee of Fudan University and the Shanghai Medical Experimental Animal Administrative Committee. All animals were bred and housed in the Department of Laboratory Animal Science of Fudan University, and all experimental procedures were conducted in accordance with the policies and ethics for animal research.

### Plasmids and cloning

Two sgRNAs (Myo6-g1: 5′-aagatgtttcaaaaggaaagTactgat-3′; Myo6-g2: 5′-aataagaagatgtttcaaaaggaaagT-3′) that targeted the $Myo6^{C442Y}$ allele and differed in their length and distance between the mutation and PAM site were tested. A gene fragment of SaCas9-KKH together with the specific sgRNA was cloned into the pX601 backbone plasmid (Addgene).

### ESC culture and transfection

The ESCs' derivation and maintenance were in ESC medium with feeder cells and cultured at 37°C in a 5% $CO_2$ atmosphere. The ESC medium was DMEM-high glucose (Millipore, SLM-220-M) supplemented with 15% (v/v) fetal bovine serum (FBS) (Gibco, 10099-141), 1× penicillin-streptomycin (Gibco, 15140-122), 1× GlutaMAX (Gibco, 35050-061), 1× MEM NEAA (non-essential amino acids) (Gibco, 11140-050), 1× 2-mercaptoethanol (Millipore, ES-007-E), 1× nucleosides (Millipore, ES-008-D), 1000 U ml$^{-1}$ LIF (Leukemia inhibitory factor), and 2i (MEK inhibitor PD0325901, 1 mM; GSK3 inhibitor CHIR99021, 3 mM).[49] For transfection, ESCs were plated onto 12-well plates and plasmids were mixed with Lipofectamine 3000 (Life Technologies) in Opti-MEM (Life Technologies) according to the manufacturer's instructions. A total of 2 μg SaCas9-KKH-Myo6-sg1/sg2/NT-sg expression plasmid was transfected into the ESCs. GFP-positive cells were sorted by fluorescence-activated cell sorting (FACS) at 48 h post-transfection.

### Mouse genomic DNA/RNA isolation and PCR

For the *in vitro* experiments, after GFP-positive ESCs were sorted by FACS, genomic DNA was isolated from the ESCs using the Quick Extract DNA Extraction Solution (Epicenter) following the manufacturer's instructions. A total of 500–1,400 ng of genomic DNA was used for NGS. Two strategies were used for the *in vivo* experiments, either the sensory epithelium was dissected at P7 and cultured for another 7 days *in vitro* or it was directly extracted from the whole cochlea soft tissue at 15 weeks after injection of the AAV-PHP.eB-SaCas9-KKH-Myo6-g2 system into the inner ear at P0–2. For RNA analysis, the RNA was extracted from the whole cochlea soft tissue at P15. Nested PCR was used for the amplification of target sites, and the PCR amplification products were purified with a Gel Extraction Kit (QIAGEN) for NGS.

### Off-target analysis

CasOFFinder software was used to predict the potential off-target sites for SaCas9-KKH-Myo6-g2, and specific primers were designed for the potential off-target sites. Off-target genomic sites were amplified from the edited genomic DNA, and the PCR products were sequenced on a MiSeq high-throughput DNA sequencer (Illumina). The primers are specified in Data S2.

### AAV virus production

The SaCas9-KKH plasmid with or without target sgRNA was sequenced before packaging into AAV-PHP.eB, and the AAV vectors were packaged by OBIO (Shanghai, China) or from Yang's lab.[28] The vector titer was $3.73 \times 10^{13}$ and $1.12 \times 10^{13}$ genome copies/mL as determined by qPCR specific for the inverted terminal repeat of the AAV-PHP.eB-SaCas9-KKH-Myo6-g2 and control virus.

### Inner ear injections

$Myo6^{C442Y/WT}$, $Myo6^{C442Y/C442Y}$, and $Myo6^{WT//WT}$ mouse pups were anesthetized by immersion in ice water at P0–2. Upon anesthesia, a post-auricular incision was made to expose the otic bulla and the stapedial artery. A total of 500 nL of AAV-PHP.eB-SaCas9-KKH-Myo6-g2 virus per cochlea was injected into the scala media through the soft cochlear lateral wall at a rate of 169 nL/min using glass micropipettes on a Nanoliter Microinjection System (WPI, Sarasota, FL, USA). The location of the basal cochlear turn is distinguished by its anatomy in relation to the stapedius artery.[23,41,50–52] After injection, a suture was used to close the incision, and the mice were placed on a 42°C heating pad for recovery. The pups were returned to their mother after they fully recovered within ~10 min. Standard post-operative care was applied after surgery.

### Hearing tests

ABR and DPOAE measurements were performed using an RZ6 Acoustic System (Tucker-Davis Technologies, Alachua, FL, USA). ABRs and DPOAEs were recorded during the same session. Mice of either sex were anesthetized with intraperitoneal injection of xylazine (10 mg/kg) and ketamine (100 mg/kg). One subcutaneous needle electrode was inserted into the subcutaneous tissues of the vertex as the reference electrode, one was inserted into the mastoid portion as the recording electrode, and one was inserted into the rump of the animal as the ground electrode. ABR potentials were evoked and subsequently amplified 10,000 times with 1,024 responses and bandpass filtered at 300 Hz–3 kHz at each sound pressure level. Tone burst sound stimuli were presented at 4, 8, 16, 24, and 32 kHz to test the frequency-specific hearing thresholds. The threshold of a certain frequency was determined as the lowest SPL at which any ABR wave could be detected upon visual inspection and could be repeated. The amplitude of wave 1 of the ABR was measured from the peak of wave 1 to the following trough.[53] The mice were placed on a heating pad covered by a sterile drape to maintain their body temperature during the testing. Data were analyzed and plotted using GraphPad Prism 8, and threshold averages ± SEM or SD are presented unless otherwise stated.

### Confocal microscopy and cell counting

We used Myosin7a as the marker for mature hair cells. The temporal bones of adult mice were harvested, cleaned, and placed in 4% formaldehyde for 1 h at room temperature, followed by decalcification for 36–72 h with 10% EDTA (pH 7.4). The sensory epithelium was then dissected and stored in PBS until staining. Tissues were permeabilized with 0.1% Triton X-100 for 1 h, blocked with 10% normal donkey serum, and then incubated with anti-MYO7A primary antibody (1:500 dilution, Proteus BioSciences) overnight, and appropriate Alexa-conjugated secondary antibodies were used for detection. DAPI was used to label the nuclei (1:1,000 dilution, Sigma). Images were acquired on a Leica TCS SP8 laser scanning confocal microscope and a 40/63× objective. Images were edited by Adobe Photoshop and the ImageJ plugin. The tools in the ImageJ software were used for counting the number of Myosin7a-positive hair cells per 100 μm length along the sensory epithelia in the apical, middle, and basal turns of the cochlea. At least two 100 μm regions from at least three independent cochleae were counted, and the results are presented as the mean ± SEM.

### Scanning electron microscopy

The temporal bones of 10-week-old adult mice were harvested, and cleaned temporal bones were placed in 2.5% glutaraldehyde in 0.1 M PBS at 4°C overnight. After the samples were sufficiently decalcified in 10% EDTA, the sensory epithelia were carefully dissected. The samples were then washed with PBS and immersed in a 1% $OsO_4$ solution in the dark for 4 h. After dehydration through an ethanol gradient, the samples were dehydrated with a critical point dryer (Samdri-795, BioCryo Tousimis) according to the manufacturer's instructions. The mounted tissues were coated with a 10 nm layer of gold (JFC-1100, Jeol, Japan), and an electron microscope (Hitachi S-4700 FESEM) was used for imaging.[9]

### Electrophysiology

To assess IHC function, we performed patch-clamp recordings in IHCs from the apical turn of the sensory epithelium from both $Myo6^{WT/WT}$ and $Myo6^{WT/C442Y}$ mice at P15–16 directly according to a protocol described previously.[54] Briefly, the apical turns of the cochlea were excised from AAV-SaCas9-KKH-Myo6-g2-treated and untreated $Myo6^{WT/C442Y}$ mice or from $Myo6^{WT/WT}$ of either sex and then bathed in an oxygenated extracellular solution containing 125 mM NaCl, 5.8 mM KCl, 5 mM $CaCl_2$, 0.9 mM $MgCl_2$, 10 mM HEPES, 5.6 mM D-glucose, 0.7 mM $NaH_2PO_4 \cdot H_2O$, and 2 mM Na-pyruvate (~290 mOsm [pH 7.2]). The tissue was visualized through a 60× water-immersion objective on an upright microscope (Olympus), and patch-clamp recordings were made through an EPC10 amplifier (HEKA Electronics, Lambrecht Pfalz, Germany) driven by the Patchmaster software (HEKA Electronics). Recording pipettes were pulled from borosilicate glass capillaries (Sutter) to a resistance of 5–6 MΩ, coated with dental wax and then filled with an intracellular solution containing 135 mM Cs-methane sulfonate, 10 mM CsCl, 10 mM TEA-Cl, 2 mM EGTA, 10 mM HEPES, 3 mM Mg-ATP, and 0.5 mM Na-GTP (~290 mOsm [pH 7.2]). All patch-clamp experiments were carried out at room temperature,

and the liquid junction potential was corrected offline. To measure $I_{Ca}$, we applied a voltage ramp from a holding potential of −90 mV to +70 mV in 0.3 s and recorded the resulting current. To measure exocytosis, we performed whole-cell $C_m$ measurements with the lock-in feature and the "Sine + DC" method in Patchmaster (HEKA). Sine waves of 1 kHz and 50 mV (peak-to-peak) were superposed onto the holding potential before and after a step depolarization (0 mV, 500 ms), and the resulting current responses were used to determine $C_m$. The net increase of capacitance before and after stimulation ($\Delta C_m$) was used to assess exocytosis of synaptic vesicles from IHCs.

### Statistical analysis

We used GraphPad Prism v.8.0 for statistical analysis. Two groups were compared using unpaired two-tailed Student's t tests. To compare more than two groups of ABRs, one-way analysis of variance (ANOVA) was performed followed by Tukey's post hoc test or Dunn's multiple comparisons test (to compare every mean to every other mean), and Holm-Sidak (or Bonferroni) post hoc analyses were performed to compare selected pairs of means. The adjusted $p < 0.05$ was considered statistically significant. At least 234 mice (P0–2) of either sex were used for injections. The mice were randomly assigned to different test groups. Data are presented as the mean ± SD or SEM as noted in the text and figure legends.

### Data and materials availability

All data and materials associated with this study are presented in the paper or the Supplemental information. Raw sequencing files have been uploaded to NCBI's Sequence Read Archive (SRA) (https://www.ncbi.nlm.nih.gov/bioproject/PRJNA684466). Information on the AAV-PHP.eB and SaCas9-KKH constructs is available from Addgene.

## AUTHOR CONTRIBUTIONS

Y.X., X.H., D.W., and D.L. designed and performed the experiments, analyzed the data, generated the figures, and wrote the manuscript.

Y.X. performed *in vivo* injections. X.H., D.W., and D.L. contributed to genome editing. Y.X., J.Z., Z.X., and X.G. contributed to hearing function experiments. F.W., Y.L., and G.L. performed the electrophysiology experiment and analyzed the data. Y.X. and J.W. contributed to confocal microscopy and SEM experiments. M.H., R.C., J.S., Z.C., and G.L. helped design the experiments, analyze the data, and write the manuscript. E.Z. and H.Y. assisted with genome editing and helped with the sequencing data analysis. Y.S., Z.C., E.Z., and H.L. conceived the project, designed and supervised the research, and wrote the manuscript. All authors reviewed, edited, and approved the manuscript.

## DECLARATION OF INTERESTS
The authors declare no competing interests.

## REFERENCES

1. Avraham, K.B., Hasson, T., Steel, K.P., Kingsley, D.M., Russell, L.B., Mooseker, M.S., Copeland, N.G., and Jenkins, N.A. (1995). The mouse Snell's waltzer deafness gene encodes an unconventional myosin required for structural integrity of inner ear hair cells. Nat. Genet. *11*, 369–375.

2. Spink, B.J., Sivaramakrishnan, S., Lipfert, J., Doniach, S., and Spudich, J.A. (2008). Long single α-helical tail domains bridge the gap between structure and function of myosin VI. Nat. Struct. Mol. Biol. *15*, 591–597.

3. Ahmed, Z.M., Morell, R.J., Riazuddin, S., Gropman, A., Shaukat, S., Ahmad, M.M., Mohiddin, S.A., Fananapazir, L., Caruso, R.C., Husnain, T., et al. (2003). Mutations of MYO6 are associated with recessive deafness, DFNB37. Am. J. Hum. Genet. *72*, 1315–1322.

4. Hasson, T., Gillespie, P.G., Garcia, J.A., MacDonald, R.B., Zhao, Y., Yee, A.G., Mooseker, M.S., and Corey, D.P. (1997). Unconventional myosins in inner-ear sensory epithelia. J. Cell Biol. *137*, 1287–1307.

5. Melchionda, S., Ahituv, N., Bisceglia, L., Sobe, T., Glaser, F., Rabionet, R., Arbones, M.L., Notarangelo, A., Di Iorio, E., Carella, M., et al. (2001). MYO6, the human homologue of the gene responsible for deafness in Snell's waltzer mice, is mutated in autosomal dominant nonsyndromic hearing loss. Am. J. Hum. Genet. *69*, 635–640.

6. Mochizuki, E., Okumura, K., Ishikawa, M., Yoshimoto, S., Yamaguchi, J., Seki, Y., Wada, K., Yokohama, M., Ushiki, T., Tokano, H., et al. (2010). Phenotypic and expression analysis of a novel myosin VI null mutant mouse. Exp. Anim. *59*, 57–71.

7. Sanggaard, K.M., Kjaer, K.W., Eiberg, H., Nürnberg, G., Nürnberg, P., Hoffman, K., Jensen, H., Sørum, C., Rendtorff, N.D., and Tranebjaerg, L. (2008). A novel nonsense mutation in MYO6 is associated with progressive nonsyndromic hearing loss in a Danish DFNA22 family. Am. J. Med. Genet. A. *146A*, 1017–1025.

8. Oka, S.I., Day, T.F., Nishio, S.Y., Moteki, H., Miyagawa, M., Morita, S., Izumi, S., Ikezono, T., Abe, S., Nakayama, J., et al. (2020). Clinical Characteristics and In Vitro Analysis of *MYO6* Variants Causing Late-Onset Progressive Hearing Loss. Genes (Basel) *11*, 273.

9. Wang, J., Shen, J., Guo, L., Cheng, C., Chai, R., Shu, Y., and Li, H. (2019). A humanized mouse model, demonstrating progressive hearing loss caused by MYO6 p.C442Y, is inherited in a semi-dominant pattern. Hear. Res. *379*, 79–88.

10. Leake, P.A., Akil, O., and Lang, H. (2020). Neurotrophin gene therapy to promote survival of spiral ganglion neurons after deafness. Hear. Res. *394*, 107955.

11. Akil, O., Seal, R.P., Burke, K., Wang, C., Alemi, A., During, M., Edwards, R.H., and Lustig, L.R. (2012). Restoration of hearing in the VGLUT3 knockout mouse using virally mediated gene therapy. Neuron *75*, 283–293.

12. Chang, Q., Wang, J., Li, Q., Kim, Y., Zhou, B., Wang, Y., Li, H., and Lin, X. (2015). Virally mediated Kcnq1 gene replacement therapy in the immature scala media restores hearing in a mouse model of human Jervell and Lange-Nielsen deafness syndrome. EMBO Mol. Med. *7*, 1077–1086.

13. Chien, W.W., Isgrig, K., Roy, S., Belyantseva, I.A., Drummond, M.C., May, L.A., Fitzgerald, T.S., Friedman, T.B., and Cunningham, L.L. (2016). Gene Therapy Restores Hair Cell Stereocilia Morphology in Inner Ears of Deaf Whirler Mice. Mol. Ther. *24*, 17–25.

14. Delmaghani, S., Defourny, J., Aghaie, A., Beurg, M., Dulon, D., Thelen, N., Perfettini, I., Zelles, T., Aller, M., Meyer, A., et al. (2015). Hypervulnerability to Sound Exposure through Impaired Adaptive Proliferation of Peroxisomes. Cell *163*, 894–906.

15. Dulon, D., Papal, S., Patni, P., Cortese, M., Vincent, P.F., Tertrais, M., Emptoz, A., Tlili, A., Bouleau, Y., Michel, V., et al. (2018). Clarin-1 gene transfer rescues auditory synaptopathy in model of Usher syndrome. J. Clin. Invest. *128*, 3382–3401.

16. Emptoz, A., Michel, V., Lelli, A., Akil, O., Boutet de Monvel, J., Lahlou, G., Meyer, A., Dupont, T., Nouaille, S., Ey, E., et al. (2017). Local gene therapy durably restores vestibular function in a mouse model of Usher syndrome type 1G. Proc. Natl. Acad. Sci. USA *114*, 9695–9700.

17. Isgrig, K., Shteamer, J.W., Belyantseva, I.A., Drummond, M.C., Fitzgerald, T.S., Vijayakumar, S., Jones, S.M., Griffith, A.J., Friedman, T.B., Cunningham, L.L., and Chien, W.W. (2017). Gene Therapy Restores Balance and Auditory Functions in a Mouse Model of Usher Syndrome. Mol. Ther. *25*, 780–791.

18. Pan, B., Askew, C., Galvin, A., Heman-Ackah, S., Asai, Y., Indzhykulian, A.A., Jodelka, F.M., Hastings, M.L., Lentz, J.J., Vandenberghe, L.H., et al. (2017). Gene therapy restores auditory and vestibular function in a mouse model of Usher syndrome type 1c. Nat. Biotechnol. *35*, 264–272.

19. Taiber, S., Cohen, R., Yizhar-Barnea, O., Sprinzak, D., Holt, J.R., and Avraham, K.B. (2021). Neonatal AAV gene therapy rescues hearing in a mouse model of SYNE4 deafness. EMBO Mol. Med. *13*, e13259.

20. Minoda, R., Miwa, T., Ise, M., and Takeda, H. (2015). Potential treatments for genetic hearing loss in humans: current conundrums. Gene Ther. *22*, 603–609.

21. Zuris, J.A., Thompson, D.B., Shu, Y., Guilinger, J.P., Bessen, J.L., Hu, J.H., Maeder, M.L., Joung, J.K., Chen, Z.Y., and Liu, D.R. (2015). Cationic lipid-mediated delivery of proteins enables efficient protein-based genome editing in vitro and in vivo. Nat. Biotechnol. *33*, 73–80.

22. György, B., Nist-Lund, C., Pan, B., Asai, Y., Karavitaki, K.D., Kleinstiver, B.P., Garcia, S.P., Zaborowski, M.P., Solanes, P., Spataro, S., et al. (2019). Allele-specific gene editing prevents deafness in a model of dominant progressive hearing loss. Nat. Med. *25*, 1123–1130.

23. Gao, X., Tao, Y., Lamas, V., Huang, M., Yeh, W.H., Pan, B., Hu, Y.J., Hu, J.H., Thompson, D.B., Shu, Y., et al. (2018). Treatment of autosomal dominant hearing loss by in vivo delivery of genome editing agents. Nature *553*, 217–221.

24. Yeh, W.H., Shubina-Oleinik, O., Levy, J.M., Pan, B., Newby, G.A., Wornow, M., Burt, R., Chen, J.C., Holt, J.R., and Liu, D.R. (2020). In vivo base editing restores sensory transduction and transiently improves auditory function in a mouse model of recessive deafness. Sci. Transl. Med. *12*, eaay9101.

25. Roux, I., Hosie, S., Johnson, S.L., Bahloul, A., Cayet, N., Nouaille, S., Kros, C.J., Petit, C., and Safieddine, S. (2009). Myosin VI is required for the proper maturation and function of inner hair cell ribbon synapses. Hum. Mol. Genet. *18*, 4615–4628.

26. Deol, M.S., and Green, M.C. (1966). Snell's waltzer, a new mutation affecting behaviour and the inner ear in the mouse. Genet. Res. *8*, 339–345.

27. Williams, L.H., Miller, K.A., Dahl, H.H., and Manji, S.S. (2013). Characterization of a novel ENU-generated myosin VI mutant mouse strain with congenital deafness and vestibular dysfunction. Hear. Res. *299*, 53–62.

28. Hu, X., Wang, J., Yao, X., Xiao, Q., Xue, Y., Wang, S., Shi, L., Shu, Y., Li, H., and Yang, H. (2019). Screened AAV variants permit efficient transduction access to supporting cells and hair cells. Cell Discov. *5*, 49.

29. Bae, S., Park, J., and Kim, J.S. (2014). Cas-OFFinder: a fast and versatile algorithm that searches for potential off-target sites of Cas9 RNA-guided endonucleases. Bioinformatics *30*, 1473–1475.

30. Heidrych, P., Zimmermann, U., Kuhn, S., Franz, C., Engel, J., Duncker, S.V., Hirt, B., Pusch, C.M., Ruth, P., Pfister, M., et al. (2009). Otoferlin interacts with myosin VI: implications for maintenance of the basolateral synaptic structure of the inner hair cell. Hum. Mol. Genet. *18*, 2779–2790.

31. Akil, O., Dyka, F., Calvet, C., Emptoz, A., Lahlou, G., Nouaille, S., Boutet de Monvel, J., Hardelin, J.P., Hauswirth, W.W., Avan, P., et al. (2019). Dual AAV-mediated gene therapy restores hearing in a DFNB9 mouse model. Proc. Natl. Acad. Sci. USA *116*, 4496–4501.

32. Askew, C., Rochat, C., Pan, B., Asai, Y., Ahmed, H., Child, E., Schneider, B.L., Aebischer, P., and Holt, J.R. (2015). Tmc gene therapy restores auditory function in deaf mice. Sci. Transl. Med. 7, 295ra108.

33. Lentz, J.J., Jodelka, F.M., Hinrich, A.J., McCaffrey, K.E., Farris, H.E., Spalitta, M.J., Bazan, N.G., Duelli, D.M., Rigo, F., and Hastings, M.L. (2013). Rescue of hearing and vestibular function by antisense oligonucleotides in a mouse model of human deafness. Nat. Med. 19, 345–350.

34. Lentz, J.J., Pan, B., Ponnath, A., Tran, C.M., Nist-Lund, C., Galvin, A., Goldberg, H., Robillard, K.N., Jodelka, F.M., Farris, H.E., et al. (2020). Direct Delivery of Antisense Oligonucleotides to the Middle and Inner Ear Improves Hearing and Balance in Usher Mice. Mol. Ther. 28, 2662–2676.

35. Nist-Lund, C.A., Pan, B., Patterson, A., Asai, Y., Chen, T., Zhou, W., Zhu, H., Romero, S., Resnik, J., Polley, D.B., et al. (2019). Improved TMC1 gene therapy restores hearing and balance in mice with genetic inner ear disorders. Nat. Commun. 10, 236.

36. Shibata, S.B., Ranum, P.T., Moteki, H., Pan, B., Goodwin, A.T., Goodman, S.S., Abbas, P.J., Holt, J.R., and Smith, R.J.H. (2016). RNA Interference Prevents Autosomal-Dominant Hearing Loss. Am. J. Hum. Genet. 98, 1101–1113.

37. Yoshimura, H., Shibata, S.B., Ranum, P.T., Moteki, H., and Smith, R.J.H. (2019). Targeted Allele Suppression Prevents Progressive Hearing Loss in the Mature Murine Model of Human TMC1 Deafness. Mol. Ther. 27, 681–690.

38. Rudman, J.R., Mei, C., Bressler, S.E., Blanton, S.H., and Liu, X.Z. (2018). Precision medicine in hearing loss. J. Genet. Genomics 45, 99–109.

39. Landegger, L.D., Pan, B., Askew, C., Wassmer, S.J., Gluck, S.D., Galvin, A., Taylor, R., Forge, A., Stankovic, K.M., Holt, J.R., and Vandenberghe, L.H. (2017). A synthetic AAV vector enables safe and efficient gene transfer to the mammalian inner ear. Nat. Biotechnol. 35, 280–284.

40. György, B., Meijer, E.J., Ivanchenko, M.V., Tenneson, K., Emond, F., Hanlon, K.S., Indzhykulian, A.A., Volak, A., Karavitaki, K.D., Tamvakologos, P.I., et al. (2018). Gene Transfer with AAV9-PHP.B Rescues Hearing in a Mouse Model of Usher Syndrome 3A and Transduces Hair Cells in a Non-human Primate. Mol. Ther. Methods Clin. Dev. 13, 1–13.

41. Shu, Y., Tao, Y., Wang, Z., Tang, Y., Li, H., Dai, P., Gao, G., and Chen, Z.Y. (2016). Identification of Adeno-Associated Viral Vectors That Target Neonatal and Adult Mammalian Inner Ear Cell Subtypes. Hum. Gene Ther. 27, 687–699.

42. Isgrig, K., McDougald, D.S., Zhu, J., Wang, H.J., Bennett, J., and Chien, W.W. (2019). AAV2.7m8 is a powerful viral vector for inner ear gene therapy. Nat. Commun. 10, 427.

43. Wang, D., Zhang, C., Wang, B., Li, B., Wang, Q., Liu, D., Wang, H., Zhou, Y., Shi, L., Lan, F., and Wang, Y. (2019). Optimized CRISPR guide RNA design for two high-fidelity Cas9 variants by deep learning. Nat. Commun. 10, 4284.

44. Kho, S.T., Pettis, R.M., Mhatre, A.N., and Lalwani, A.K. (2000). Safety of adeno-associated virus as cochlear gene transfer vector: analysis of distant spread beyond injected cochleae. Mol. Ther. 2, 368–373.

45. Zuo, E., Sun, Y., Wei, W., Yuan, T., Ying, W., Sun, H., Yuan, L., Steinmetz, L.M., Li, Y., and Yang, H. (2020). GOTI, a method to identify genome-wide off-target effects of genome editing in mouse embryos. Nat. Protoc. 15, 3009–3029.

46. Zuo, E., Sun, Y., Wei, W., Yuan, T., Ying, W., Sun, H., Yuan, L., Steinmetz, L.M., Li, Y., and Yang, H. (2019). Cytosine base editor generates substantial off-target single-nucleotide variants in mouse embryos. Science 364, 289–292.

47. Ehret, G. (1976). Development of absolute auditory thresholds in the house mouse (Mus musculus). J. Am. Audiol. Soc. 1, 179–184.

48. Hall, J.W., 3rd (2000). Development of the ear and hearing. J. Perinatol. 20, S12–S20.

49. Czechanski, A., Byers, C., Greenstein, I., Schrode, N., Donahue, L.R., Hadjantonakis, A.K., and Reinholdt, L.G. (2014). Derivation and characterization of mouse embryonic stem cells from permissive and nonpermissive strains. Nat. Protoc. 9, 559–574.

50. Wang, Y., Sun, Y., Chang, Q., Ahmad, S., Zhou, B., Kim, Y., Li, H., and Lin, X. (2013). Early postnatal virus inoculation into the scala media achieved extensive expression of exogenous green fluorescent protein in the inner ear and preserved auditory brainstem response thresholds. J. Gene Med. 15, 123–133.

51. Yu, Q., Wang, Y., Chang, Q., Wang, J., Gong, S., Li, H., and Lin, X. (2014). Virally expressed connexin26 restores gap junction function in the cochlea of conditional Gjb2 knockout mice. Gene Ther. 21, 71–80.

52. Gu, X., Wang, D., Xu, Z., Wang, J., Guo, L., Chai, R., Li, G., Shu, Y., and Li, H. (2021). Prevention of acquired sensorineural hearing loss in mice by in vivo Htra2 gene editing. Genome Biol. 22, 86.

53. Bramhall, N.F., Niemczak, C.E., Kampel, S.D., Billings, C.J., and McMillan, G.P. (2020). Evoked Potentials Reveal Noise Exposure-Related Central Auditory Changes Despite Normal Audiograms. Am. J. Audiol. 29, 152–164.

54. Liu, H., Lu, J., Wang, Z., Song, L., Wang, X., Li, G.L., and Wu, H. (2019). Functional alteration of ribbon synapses in inner hair cells by noise exposure causing hidden hearing loss. Neurosci. Lett. 707, 134268.